Biophysical Journal Volume 102 May 2012 2279–2287

Hydrophobic Mismatch and Lipid Sorting Near OmpA in Mixed Bilayers: Atomistic and Coarse-Grained Simulations

Fuchang Yin and James T. Kindt*
Department of Chemistry, Emory University, Atlanta, Georgia

ABSTRACT To understand the effects of lipid composition on membrane protein function in a mixture as complex as a biomembrane, one must know whether the lipid composition local to the protein differs from the mean lipid composition. In this study, we simulated the transmembrane domain of a β-barrel protein, OmpA, in mixtures of lipids of different tail lengths under conditions of negative hydrophobic mismatch, i.e., local bilayer thinning. We modeled the influence of OmpA on the local lipid composition both at a coarse-grained (CG) resolution using conventional molecular dynamics, and at an atomistic resolution within the semi-grand canonical ensemble using mutation moves to rapidly approach an equilibrium lateral distribution of lipids. Moderate enrichment of the shorter tail component (either DDPC in DDPC/DMPC mixtures or DMPC in DMPC/DSPC mixtures) extending 2–3 nm away from the protein surface was observed with both the atomistic and CG models. The similarity in trends suggests that the more computationally economical CG models capture the essential features of lipid sorting induced by hydrophobic mismatch.

INTRODUCTION

Biological membranes are complex assemblies composed of a large variety of lipids, proteins, and other molecules. The hydrophobic interaction between the lipid acyl tails and hydrophobic residues on protein transmembrane domains is an important factor in determining the structure of membrane proteins and their organization within the bilayer, which consists of a hydrophobic interior sandwiched between two hydrophilic water interfaces. The pattern of hydrophilic and hydrophobic surfaces exposed by a single transmembrane segment dictates where these surfaces will reside in the bilayer structure. When the hydrophobic length of the protein segment is less than the hydrophobic thickness of the bilayer, local thinning of the bilayer is expected to accommodate this negative hydrophobic mismatch. Recent reviews (1–3) summarize experimental and theoretical studies that examined how changes to the bilayer thickness and protein tilt, along with other possible accommodations, allow the bilayer and protein to act together to optimize their interactions.

In a bilayer with more than one lipid type, spatial variations in composition may result from these perturbations (4). Experimental efforts over the last few decades have aimed to measure the degree of enrichment of lipid components of varying tail lengths near a protein embedded in a mixed bilayer. This effect is clear when the bilayer lipids themselves spontaneously demix into phases with different compositions, and the protein partitions selectively to one phase (5–7). Within homogeneous fluid-phase mixtures, evidence for lipid sorting has been less clear. Using fluorescence resonance energy transfer, Dumas et al. (5) were unable to distinguish any enrichment of dilauroylphosphatidylcholine (DLPC, i.e., 12:0/12:0 PC) near bacteriorhodopsin in fluid-phase DLPC/distearoylphosphatidylcholine (DSPC, i.e., 18:0/18:0 PC) mixtures, in contradiction to predictions of MC simulations. Photo-cross-linking of a chemically modified WALP23 helical peptide in fluid-phase lipid mixtures under hydrophobic mismatch conditions yielded a statistical mixture of long- and short-tailed lipid neighbors, with no apparent enrichment of either species (6). Caffrey and Feigenson (7) used fluorescence quenching to derive binding constants to the Ca^{2+} ATPase transmembrane protein for a variety of PC lipids with different tail lengths and degrees of saturation, and found a range of 0.90–1.45 (relative to dioleoylphosphatidylcholine (DOPC), i.e., 18:1/18:1 PC). More recently, other investigators (8–11) used a similar approach to study a variety of transmembrane peptides and proteins, and found relative binding constants (also relative to DOPC) as large as 2.4 and as small as 0.4 for lipids of varying tail length. For a review and analysis of these and related studies, see Marsh (12).

Because of the slow lateral diffusion rate of lipids in bilayers, molecular-dynamics (MD) simulations need to reach the microsecond timescale to ensure that a mixture of lipids will sample a representative equilibrium ensemble of lateral distributions. This is readily achievable with the use of coarse-grained (CG) models. Nielsen et al. (13) simulated mismatch-induced sorting effects using a CG mixed-lipid bilayer with a smooth cylinder representing the peptide, and observed local enrichment of the shorter lipid, better matched to the peptide, after 1 ns of MD simulation. Klingelhoefer et al. (14) studied the distribution of lipid in two component lipid bilayers containing α-helix bundle and β-barrel peptides, using the MARTINI force field, and found lipid sorting consistent with the effects of hydrophobic mismatch (15).

Submitted November 20, 2011, and accepted for publication April 4, 2012.
*Correspondence: jkindt@emory.edu
Editor: Scott Feller.

0006-3495/12/05/2279/9 $2.00
doi: 10.1016/j.bpj.2012.04.005

Simulations with atomistic detail are $\geq$10-fold more computationally expensive than CG simulations, which makes atomistic studies of lipid lateral distributions through conventional MD simulation time-consuming. Atomistic simulations are nonetheless important, especially because CG models like MARTINI are typically parameterized to match single-component bilayer properties, and thus the realism of their performance within mixtures needs to be established in benchmark calculations with atomistic lipid models. To overcome the limitation of conventional MD, we use a Monte Carlo (MC)-MD approach that allows mutations between long- and short-tailed lipids by attempting configurational bias Monte Carlo mutation moves within the isomolar semigrand canonical ensemble. The temperature, pressure, surface tension, and total number of lipids are fixed, whereas the lipid composition fluctuates under the influence of a constant difference $\Delta\mu$ between chemical potentials of the two lipid components (16,17). In a system containing a peptide embedded in a lipid bilayer, the distribution of different types of lipid as a function of distance from the peptide can be monitored over a trajectory in which the lipids undergo mutations. Because all lipids in the system are coupled to the same virtual reservoirs of the two components, the distribution of the two lipid types throughout the system converges to an equilibrium lateral distribution. In a previous study (18), this technique was applied to gramicidin-A (GCA) peptide in DMPC-DDPC (didecanoyl-L-α-phosphatidylcholine, 10:0/10:0 PC) and DSPC-DMPC mixed lipid bilayers. Although local thinning and thickening effects on the bilayer were notable in the simulations, only weak hydrophobic sorting was evident, as the local composition was perturbed $<$5% from the mean. The noncylindrical (hourglass) shape of GCA may tend to confound any tendency toward sorting associated with thickness distortions.

Here we consider hydrophobic mismatch-induced lipid sorting around a larger β-barrel peptide, the transmembrane domain of *Escherichia coli* outer membrane protein A (OmpA) (19). The greater diameter of this peptide (relative to GCA) tends to suppress its tilting with respect to the bilayer normal and leads to more numerous nearest neighbors, which in turn allows better statistical sampling of their mean composition. Furthermore, a generic β-barrel protein of similar size was used in previous CG simulations that demonstrated lipid sorting (14). In the work presented here, we used both CG and atomistic models to simulate the interaction of OmpA with lipid bilayers representing 1:1 mixtures of the saturated tail lipid DMPC with analogs with tails that were either shorter or longer by four methylene groups per tail (DDPC and DSPC, respectively).

METHODS

CG model simulations

We performed conventional MD simulations using the MARTINI CG force field (15,20) and Gromacs 4 (21) with the MD integration time step set to 25 fs at a temperature of 298 or 330 K. The elastic network model (22) was applied to OmpA to maintain a conformation close to the experimental x-ray crystal structure (19) over long trajectories. Periodic boundary conditions were applied in three dimensions, with semi-isotropic pressure coupling using the Berendsen barostat (23) at 1 bar at a coupling constant of 1.0 ps and a compressibility of 1×10^{-4} bar.

To construct systems for simulation, we chose three CG lipid species (CG5, CG4, and CG3, approximating DSPC, DMPC, and DDPC) that consist of the same PC headgroup, and three, four, and five CG fatty acyl chain beads, respectively. For each system size, we studied five lipid environments: pure CG5, pure CG4, pure CG3, and a 1:1 mixture of CG5-CG4 or CG4-CG3. We engineered the lipid bilayer by duplicating a pair of lipids in a tail-to-tail configuration in the lateral direction. After inserting the OmpA peptide into the middle of the engineered pure bilayer, we removed the overlapping lipid pairs and obtained a square box with OmpA in the middle. We added CG water by using the Gromacs *genbox* tool. We prepared three systems of different sizes, each with 1 OmpA but varying amounts of lipid: 558 lipids with 11,581 CG water, 200 lipids with 1500 CG water, and 128 lipids with 1500 CG water. We obtained a mixed system from the pure system by randomly changing half of CG5 to CG4 for the CG5-CG4 mixture (or CG4 to CG3 for the CG4-CG3 mixture) on each lipid monolayer. After a brief initial equilibration to eliminate the vacancies associated with the particle removal, we performed 2000 ns of conventional MD simulation for each system.

Atomistic (united-atom) model simulations

Starting configurations for atomistic simulations of OmpA-containing bilayers were obtained from CG structures with the use of a reverse CG procedure. Five CG systems containing 128 lipids (all CG5, 1:1 CG5:CG4, all CG4, 1:1 CG4:CG3, and all CG3) plus one OmpA peptide were prepared and equilibrated as described above for 1000 ns. Atomistic model coordinates were generated from the final CG coordinates using the package developed by Rzepiela et al. (24). In the transformation, a one-to-many particle map was generated for each molecule type. In the configuration presented here, the DDPC, DMPC, and DSPC lipids, which have 10, 14, and 18 carbons per acyl tail, respectively, are modeled by CG3, CG4, and CG5, respectively.

In the atomistic simulations, we used a combination of the protein OPLS-AA (all-atom) force field (25) with the united-atom (UA) lipid force field of Berger et al. (26) and the TIP3P model (27) of water, as suggested by Tieleman et al. (28). We used a Langevin thermostat (29) with a time constant of 0.1 ps to maintain a constant temperature of 330 K in all simulations. A Berendsen barostat (23) was used for semi-isotropic pressure scaling (at 1 bar pressure, zero surface tension, and time constant of 1.0 ps at assumed compressibility 4.5×10^{-5} bar^{-1}), and the particle-mesh Ewald method was used for electrostatic forces calculated during the MD step (30). A time step of 2 fs was used, and the SETTLE (31) and LINCS (32) algorithms were used to constrain all bonds to fixed lengths. We performed 60 ns of conventional MD simulation for each of the five reverse-CG starting structures, and the final 20 ns of the pure systems were used for comparison with the mixtures.

Mixed MC-MD simulations

We performed MC-MD simulations using GIMLi 1.0, a customized version of Gromacs 3.3, to study the two-component lipid bilayer with embedded peptide. As detailed elsewhere (16,17), we used a constant ratio of thermodynamic activities of the two lipid components to control the composition of lipids. The activity ratio α can be represented in terms of the chemical potential difference as $\alpha = \exp(\Delta\mu/k_BT)$, where $\Delta\mu = \mu_{DSPC} - \mu_{DMPC}$ (or $\mu_{DMPC} - \mu_{DDPC}$). We chose values of α that in previous studies (18) were shown to yield nearly 1:1 mixtures of the two components in a protein-free system. During MC-MD simulations, after every MD time

step, we randomly chose a lipid and subjected it to a mutation move attempt (shortening its tail if it was a long-tailed lipid, and extending it if it was a short-tailed lipid) using the configuration-bias algorithm (33). The mean success rate was ~0.25%, or one lipid mutation event in the system every 0.8 ps; on average, each lipid underwent one mutation per 100 ps.

Analysis

In both the CG and atomistic models, bilayer thickness and lipid distribution were measured as a function of distance from the center of mass of the peptide. To analyze these quantities, we used the NC3 site for CG simulations and the phosphorus atom for the UA simulations. The radius interval was 0.1 nm. Counts of particles and average position were summed over each interval and all time frames, divided by the number of frames, and normalized. Thickness is defined as the difference in the mean z coordinate of reference particles in the upper and lower leaflets falling in the same radial bin. Lipid composition was evaluated as the mean number of lipid reference sites of each type (summed over both leaflets) in each radial bin divided by the bin area, which was then converted into a mole % of the longer-tail component.

We analyzed the protein structure root mean-square deviation (RMSD) over MD trajectories relative to the crystal structure using the trajectory tool of VMD (34). Comparisons were made either between the entire set of backbone sites or between Cα carbons of the following subset of 90 residues that occupy a 2.8-nm range along the barrel axis, excluding the loops on the membrane exterior side: 7–12, 14–17, 36–47, 50–59, 76–82, 85–87, 92–103, 120–133, 136–145, and 161–171.

RESULTS AND DISCUSSION

CG model simulations

The introduction of OmpA into lipid bilayers over a range of thicknesses from ~12 to ~20 carbons per chain, as simulated with a CG model, produces thinning of the bilayer by up to 1 nm near the peptide, as shown in Fig. 1. The degree of thinning and the area extent of the region thinned are expected to be governed by the area compressibility and curvature moduli of the bilayer (35), which have been shown to have reasonable values within the MARTINI force field (20,36). The bilayer thickness, starting at the β-barrel external edge at 1.5 nm, monotonically increases with distance until 3–4 nm and then levels off. The thickness at short range increases with the bilayer tail length, consistent with the calculations of Marsh (12), indicating that the thickness accommodation falls short of reaching perfect matching at contact. In the case of the pure CG3 bilayer, the thickness reaches a maximum at a distance of 3.0 nm and drops very gradually beyond that. Such a nonmonotonic thickness profile was previously explained in terms of monolayer spontaneous curvature effects (37).

Fig. 2 shows the radial distribution of lipids of the mixtures. A clear lipid sorting effect was observed for both mixtures at all system sizes, indicating that in each case the lipid with greater hydrophobic mismatch (i.e., the longer one) is depleted near the OmpA peptide. The effect is similar in magnitude to previously reported lipid sorting in CG simulations of an idealized α-helical bundle (14). The radius of the depleted region extends to 4.5 nm away from the center of the peptide, well beyond the first layer

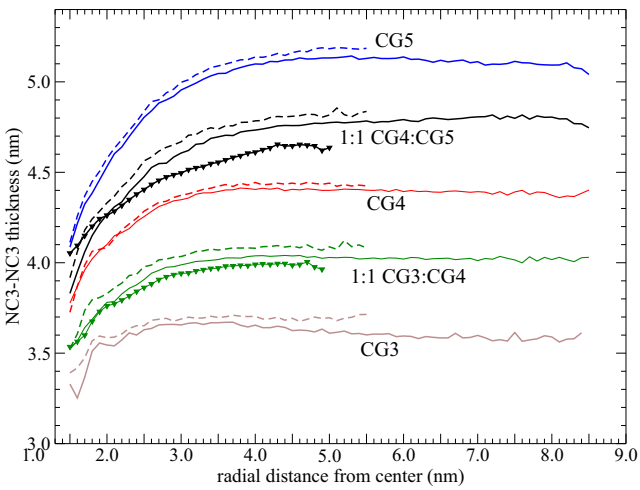

FIGURE 1 Lipid bilayer thickness in CGn simulations at 298 K (where n denotes the number of CG particles in the lipid tails, calculated as described in Materials and Methods). From top to bottom, curves represent CG5, 1:1 CG5:CG4, CG4, 1:1 CG4:CG3, and CG3 systems. Solid curves represent larger systems (558 lipids), dashed curves represent smaller systems (200 lipids), and solid symbols represent the smallest systems (128 lipids).

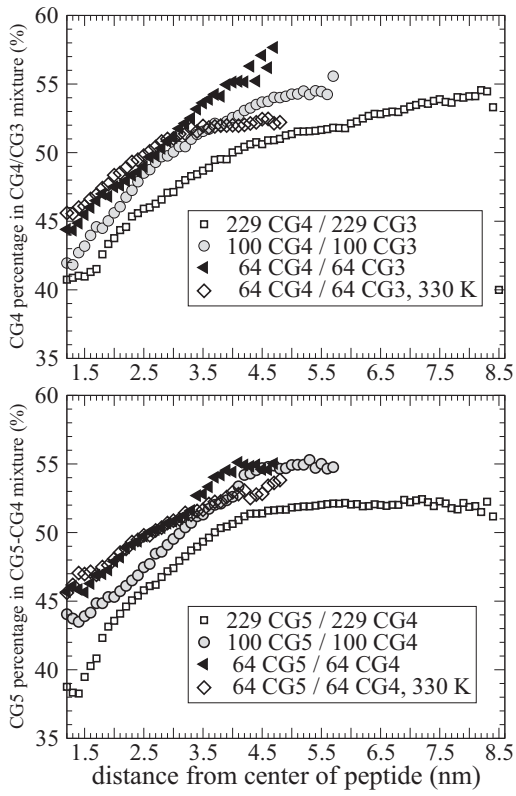

FIGURE 2 Lipid composition (% long-tailed lipid) versus lateral distance from OmpA in CG simulations of 1:1 lipid mixtures (at 298 K except where otherwise specified) determined as described in Materials and Methods. Upper panel: Mixtures of CG3 and CG4 CG lipids. Lower panel: Mixtures of CG4 and CG5 CG lipids.

of lipids. Because the system dimensions are comparable or lower than the depletion range, the percentage of long-tailed lipid immediately near the peptide is dependent on the lipid/peptide ratio between 128 and 500 lipids at fixed total lipid composition. This result stands in contrast to the experimental determination by Powl et al. (11) that the apparent relative binding coefficient of lipids of varying tail lengths to the helical bundle MscL does not depend on a lipid/peptide ratio above 50:1 up to 500:1. This discrepancy may be due to factors specific to the particular protein, or to shortcomings of the MARTINI force field. More likely, differences between the lateral distribution of peptides in the simulation (evenly spaced in a square lattice) and experiment (where peptides may cluster together) may account for this difference. Aggregation into clusters of proteins separated by one or two lipid neighbors would shield most boundary lipids from effects of the bulk. Attractions mediated by hydrophobic mismatch effects have been predicted theoretically (12,38) and observed in experiments (39). Protein clusters arising from these forces were observed in recent CG model simulations (40,41), even at a lipid/peptide ratio $>$ 400:1 (41).

A stronger bilayer thickness perturbation was noted for the CG4-CG5 mixture than for the CG3-CG4 mixture; however, the degree of sorting in the two mixtures is very similar. This similarity is consistent with the linear dependence of the free-energy penalty with hydrophobic mismatch found experimentally (12), but in contrast to the quadratic dependence predicted based purely on membrane elasticity (42).

UA simulations

Given the widespread interest in using CG models for lipid simulations, it is useful to make a direct comparison between the CG model and atomistic model descriptions of lipid mixing and demixing. We first generated starting structures for the atomistic simulations, containing pure lipids or 50:50 mixtures, from CG model configurations as described in Materials and Methods, and then equilibrated them using conventional MD for 60 ns. Fig. 3 shows the snapshots of the simulated β-barrel peptide and the peptide embedded in a DMPC-DSPC lipid bilayer. As with the CG model, plots of bilayer thickness versus distance from the peptide show a local thinning effect as expected for a negative hydrophobic mismatch, evident in Fig. 4. The trajectory initiated with a 50:50 DDPC/DMPC mixture is an exception to this trend. Inspection of the structure in this case shows that an undulation of the bilayer obscures local thinning, because the projected thickness associated with a locally tilted bilayer is greater than the actual thickness.

We used the MC-MD method to sample lipid distributions efficiently in both lipid mixtures. To test the sensitivity of the results on initial conditions, we performed three simulations in each case: two with initial compositions of 100% of one lipid or the other, and one starting with a 1:1 mixture. Because both lipid mutations and lipid/protein rearrangements require sufficient time to reach a new equilibrium, we reserved the first 20 ns of MC-MD for equilibration, and analyzed lateral distributions over the subsequent 40 ns.

MC-MD simulation trajectories of both lipid mixtures without peptide, lasting 40 ns, were performed at activity ratios that match the peptide-containing runs. The mean composition obtained in these control simulations is a useful reference point. Control systems represent regions of bilayer that are removed from the influence of any peptides but are able to exchange lipids with the peptide-containing bilayers through their common coupling to ideal reservoirs with the same lipid activity ratio. If the presence of the peptide has a more favorable free-energy effect on one lipid than on the other (i.e., increases its chemical potential by a lower amount, or decreases it by a greater amount), then the mole fraction of that lipid in the peptide-containing system must exceed its mole fraction in the control system for the two systems to satisfy the constraint of equal $\Delta\mu$ dictated by the ensemble. The mean lipid compositions obtained for all MC-MD runs are given Table 1. In two of the three DMPC-DDPC/OmpA systems, the percentage of the longer-tailed lipid (DMPC) is below the range of uncertainties of the controls, indicating that the peptide has a

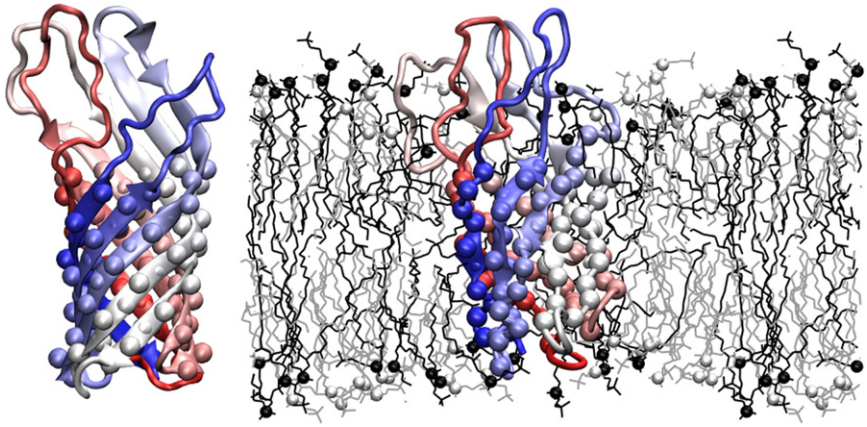

FIGURE 3 Structure of OmpA in crystal state (*left*) and embedded in a mixed DMPC-DSPC bilayer from atomistic MC-MD simulation, trajectory P-MS2. Cα carbons used to define the core of the barrel are shown as spheres in both cases. Bilayer-embedded peptide is shown with lipids as lines, with small spheres marking the P atom site (DSPC in *black*, DMPC in *gray*). Lipids are cut away to reveal peptide, and solvent is omitted.

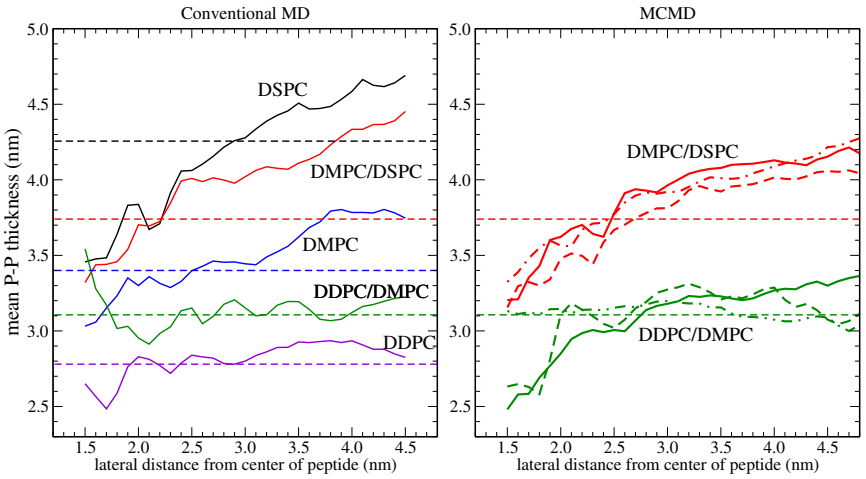

FIGURE 4 Bilayer thickness as a function of lateral distance from OmpA peptide from UA simulation, calculated as described in Materials and Methods. The left panel shows the thickness averaged over final 40 ns of MD equilibration period for single-component systems and 1:1 mixtures; solid curves represent systems containing OmpA, and dashed horizontal lines represent the average thickness of control, peptide-free bilayers. The right panel shows the thickness averaged over final 40 ns of MC-MD simulation for DMPC/DSPC mixtures (*upper group*) and DDPC/DMPC mixtures (*lower group*). Solid curves: P-MS1 and P-DM1 (starting compositions all shorter-tailed lipids); dashed curves: P-MS2 and P-DM2 (starting compositions all longer-tailed lipids); and dot-dashed curves: P-MS3 and P-DM3 (starting compositions 50/50 mixtures). Horizontal dashed lines in each case give the mean thickness of the peptide-free bilayer at the same activity ratio.

greater affinity for the shorter-tailed component (as expected given the local thinning). In the system initiated with a 50/50 mixture of the two lipids, where on average no thinning effect was seen, the presence of the peptide leaves the overall composition unaltered. In the DSPC-DMPC mixture, the average DSPC percentage of the control systems is 48.7%. With embedded OmpA peptide, the DMPC percentage varies from 46.4% to 48.7%, which is 0–2.3% lower than the control runs. From these limited samples, we estimate that OmpA will recruit on average an excess of 2.5 DDPC in a 1:1 DMPC/DDPC mixture, or 1.8 DMPC molecules in a 1:1 DSPC/DMPC mixture.

The percent uncertainties in equilibrium composition given in Table 1 were calculated from the total number of successful mutations in each trajectory as described previously (43), based on the assumption of uncorrelated, stochastic, uniform mutation rates for all lipids. Agreement in composition among control trajectories with different initial compositions was consistent with these estimates. In contrast, variability in composition among the peptide-containing systems exceeded these uncertainty ranges. The likely explanation is that specific peptide conformations lead to different microenvironments for the lipids to explore, and that transitions among these different protein structures are slow on the 40-ns simulation timescale. In fact, qualitative differences among peptide conformations are readily apparent from simulation snapshots, as shown in Fig. 5. The peptide retained a cylindrical structure in all cases, but the barrel radius and dimension and the order of the β-sheet structure departed from the x-ray crystal structure and varied among trajectories. Loop conformations showed even greater variability. RMSDs from the crystal structure, averaged over the last 20 ns of MC-MD simulation, are given in Table 2 for both the entire peptide backbone and for a subset of 90 Cα carbons that form the core of the β-barrel. This variability in protein structure was present during the MD equilibration period and is not an artifact of the MC-MD method. In two cases (P-DM1 and P-MS3), the barrel expanded to the point that it accommodated a column of water several molecules thick, allowing ready diffusion across the bilayer. A further variation occurred in the DMPC/DDPC simulation initiated with 100% DMPC, which (4 ns after the start of MC-MD simulations) developed a lipidic water pore, with dynamic involvement of three to four lipid headgroups, outside of the barrel. Our simulations were performed at 330 K, unlike previous simulation studies on OmpA conducted at 310 K (44), where the protein retained more order and did not

TABLE 1 MC-MD trajectory conditions and mean lipid compositions obtained

Code	Initial composition	System	Activity ratio	Long-tailed lipids %
C-DM1	all DDPC	DD/DM	4.00×10^{-4}	51.4 ± 0.2
C-DM2	all DMPC	DD/DM	4.00×10^{-4}	51.0 ± 0.2
P-DM1	all DDPC	DD/DM, OmpA	4.00×10^{-4}	48.5 ± 0.2
P-DM2	all DMPC	DD/DM, OmpA	4.00×10^{-4}	48.4 ± 0.2
P-DM3	1:1 DMPC/DDPC	DD/DM, OmpA	4.00×10^{-4}	50.9 ± 0.2
C-MS1	all DMPC	DM/DS	3.87×10^{-4}	48.6 ± 0.2
C-MS2	all DSPC	DM/DS	3.87×10^{-4}	48.9 ± 0.2
P-MS1	all DMPC	DM/DS, OmpA	3.87×10^{-4}	46.4 ± 0.2
P-MS2	all DSPC	DM/DS, OmpA	3.87×10^{-4}	48.7 ± 0.2
P-MS3	1:1 DSPC/DMPC	DM/DS, OmpA	3.87×10^{-4}	47.0 ± 0.2

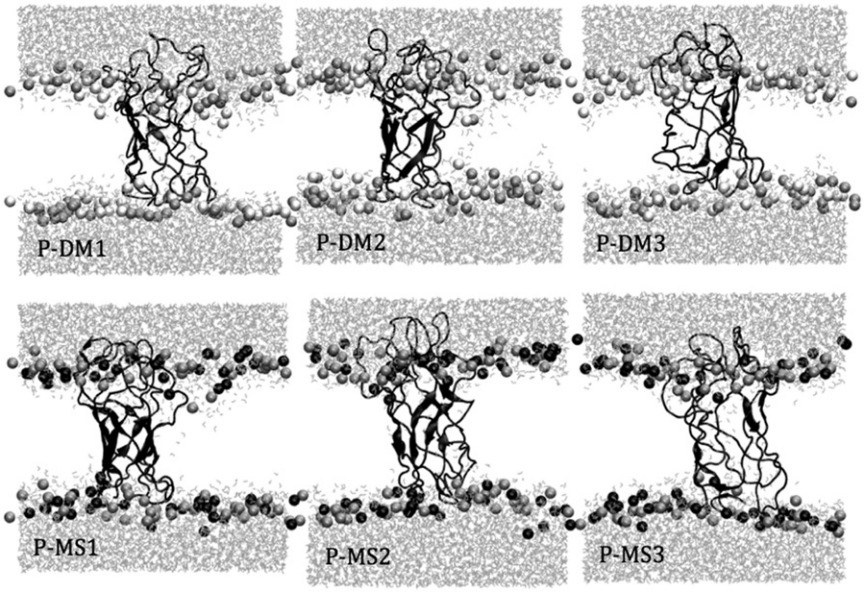

FIGURE 5 Final structures of OmpA-containing mixed-lipid bilayers. Only the phosphorus site is shown for the lipids (*white*, DDPC; *gray*, DMPC; *black*, DSPC) to expose the protein and solvent structure. Trajectory labels follow definitions in Table 1.

spontaneously undergo a transition to a solvent-filled pore. The lack of consensus in protein structure among the different trajectories makes it difficult to glean definitive insights into OmpA's biological function as a porin (45) because we cannot assess the stability of these structures beyond the 60-ns timescale. The variability of OmpA structure in these simulations may be related to the tendency (inferred from folding experiments) for bilayers thinner than DMPC to produce partially misfolded (but bilayer-embedded) intermediates (46), or to the observation that distinct, long-lived states of OmpA exhibit markedly different conductivities (47). We note, however, that some authors have attributed transitions between high- and low-conductivity states of OmpA to the involvement of an extracellular domain that is not included in our model (48).

Despite the structural variations of the OmpA peptide in the different trajectories, with one exception (noted above) they show similar local thinning effects (Fig. 4), and the correlation between local thinning and local enrichment of the shorter-tailed lipid can still be addressed. The local thickness increases from 3.2 nm at 1.5 nm distance to 4.1 nm at 4.5 nm distance in the DMPC/DSPC mixture. This thickness increase of 0.9 nm is roughly twice what was seen for the same mixture containing embedded GCA (18). In two of the three DDPC/DMPC mixture trajectories, the thickness increased from 2.6 nm to 3.2 nm over the same 3-nm distance range. The trajectory that initiated as a 50/50 mixture showed no local thinning and continued the anomalous behavior it showed during the MD equilibration period. The radial distributions of lipid types as a function of distance from the center of OmpA peptide for both mixtures are shown in Fig. 6. CG system compositions (from Fig. 2) are also included for reference. For DMPC/DDPC mixtures in the range of 2.5–4.5 nm away from the peptide, there is qualitative agreement among the three atomistic simulation trajectories and the CG model trajectory: all show modest increases in the fraction of the longer-tailed component with increasing distance from the peptide. Closer to the peptide, the compositions observed in different trajectories diverge as a result of both statistical noise (due to the smaller total number of lipids per unit distance) and variability in protein conformation. The trajectory that initiated with 100% DDPC gave results similar to those obtained in the CG model systems, with modest local depletion of the longer-tailed lipid near the peptide. The trajectory starting from 100% DMPC, in which

TABLE 2 RMSD difference between simulated OmpA conformations in MC-MD trajectories and the experimental crystal structure of Pautsch and Schulz (19), calculated using the trajectory analysis tool of VMD (34)

Trajectory	Description	RMSD, Å (all backbone)	RMSD, Å (barrel core)
P-DM1	DDPC/DMPC, from 100% DDPC	8.9 ± 0.3	4.6 ± 0.2
P-DM2	DDPC/DMPC, from 100% DMPC	6.2 ± 0.1	3.2 ± 0.1
P-DM3	DDPC/DMPC, from 50/50 mixture	6.8 ± 0.1	3.9 ± 0.1
P-MS1	DMPC/DSPC, from 100% DMPC	6.1 ± 0.2	3.2 ± 0.1
P-MS2	DMPC/DSPC, from 100% DSPC	4.7 ± 0.1	3.0 ± 0.1
P-MS3	DMPC/DSPC, from 50/50 mixture	7.9 ± 0.4	4.4 ± 0.4

Barrel-core values only include a set of 90 Cα sites that remained embedded in the bilayer over all simulations (see Materials and Methods). All-backbone values include backbone sites on all residues including loops.

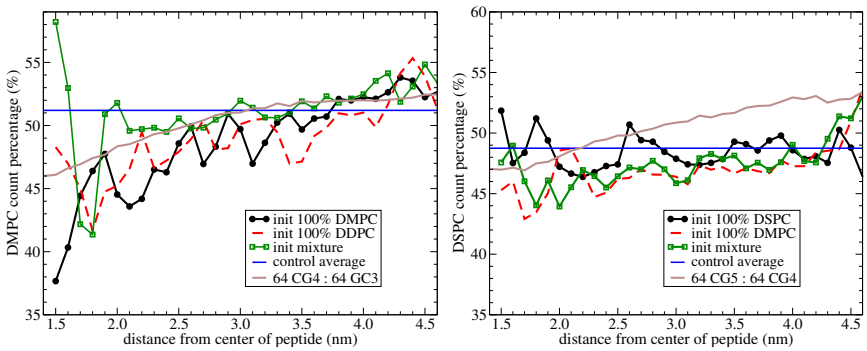

FIGURE 6 Lipid radial distribution from MC-MD simulations for DDPC-DMPC (*left*) and DMPC-DSPC (*right*) mixtures. The three trajectories are indicated by symbols as described in the figure. Horizontal lines give the average composition from control (peptide-free) MC-MD simulations. Gray curves represent the corresponding CG mixtures containing 128 lipids at 330 K (duplicate of data from Fig. 2).

a lipidic pore opens up, shows even greater depletion of the longer-tailed lipid near the peptide. In this case, it is difficult to disentangle the effect of the pore from the effect of the peptide. The trajectory that started with a 50:50 mixture, in which there was a pronounced undulation in the bilayer near the peptide and no local thinning, showed no local depletion of DMPC.

DSPC/DMPC mixtures, where the stronger local thinning trend might be expected to correlate with more pronounced lipid sorting, showed a trend with a weaker slope than either the DMPC/DDPC mixtures or the CG simulations in two of three trajectories. The trajectory that initiated with 100% DSPC did not show any consistent trend in composition versus distance from the peptide.

Given that the structure of OmpA is not symmetric about the barrel axis, it is possible that the local composition can vary axially as well as radially with respect to the protein position; composition variations could be determined by consistent interactions with specific residues on the surface, or by thickness differences around the protein surface as observed in a larger β-barrel system (49). Two-dimensional distributions of excess density of short-tailed lipid, averaged over the production period, are shown in Fig. S1 of the Supporting Material, with gray pixels representing the position distribution of the Arg-169 Cα site chosen as a reference point. These plots are complementary to Fig. 6. Clearly, they show angle-resolved composition. Additionally, by giving an absolute excess concentration rather than a local percentage, they avoid exaggerating small random fluctuations in regions where lipid density is very low. There is no particular conserved pattern to the composition as a function of direction around the pore with respect to the Arg-169 reference point. Nonetheless, the immediate neighborhood of the protein is marked by the greatest magnitude composition fluctuation in both directions. The existence of these hot spots points to poorer sampling of lipids near the protein, due to the stronger conformational constraints imposed by interactions with the protein compared with other lipids.

Perturbation to the membrane from hydrophobic mismatch is expected to influence tail ordering. The mean absolute order parameters, $|S_{CD}| = |(3<\cos^2\theta>-1)/2|$ (where θ is the angle between the C-H bond and the bilayer normal, inferred from the acyl backbone geometry in this UA model) along the lipid tails for all mixtures are shown in Fig. 7. The influence of the protein on order parameter is consistent with expectations based on the thickness profiles of Fig. 4. Bilayer thinning in the DDPC/DMPC system is associated with lowering of the order parameters. The one system that displays a water pore external to the protein (open squares) shows significantly lower DDPC order than the two other trajectories at the same composition, highlighting the importance of DDPC in creating and stabilizing that defect. As shown in Fig. 4, thinning of the DMPC/DSPC systems near the peptide is counterbalanced by a thickening at distances > 2.5 nm. Because the latter region represents a majority of the lipid area of the system, a net average thickening effect from OmpA is accompanied by a weak increase in tail order. This result highlights a potential pitfall in relying on the tail order parameter (or other averaged

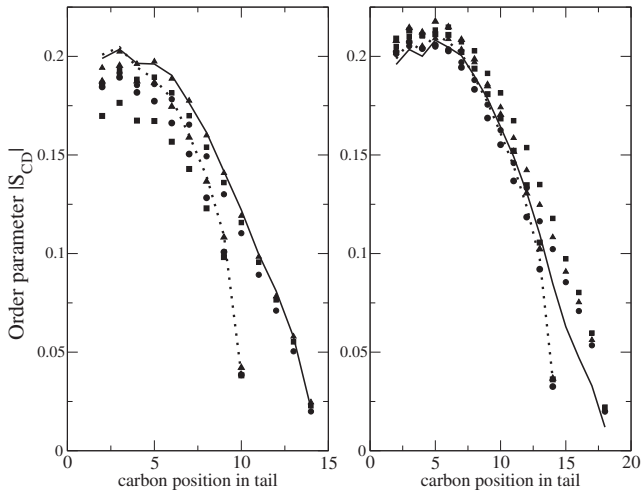

FIGURE 7 Average C-H bond order parameter profile for DDPC/DMPC mixtures (*left panel*) and DMPC/DSPC mixtures (*right panel*). Symbols represent systems containing OmpA: circles, trajectories initiated with 100% short-tailed lipid; squares, initiated with 100% longer-tailed lipid; triangles, initiated with 50/50 mixture. Open symbols indicate shorter-tailed lipid. Solid and dotted lines represent longer- and shorter-tailed lipids, respectively, in control (no-peptide, mixed-lipid) simulations.

indicators of bilayer thickness) to assess lipid response to hydrophobic mismatch: an intermediate range thickening can overcome a thinning effect immediately adjacent to a protein.

CONCLUSIONS

In this work, we simulated the OmpA transmembrane domain β-barrel peptide in lipid bilayers using atomistic and CG models. The CG model with three, four, or five particles (CG3, CG4, and CG5, respectively) shows a strong system size dependence on hydrophobic sorting at fixed lipid composition, indicating that a lipid/peptide ratio of at least 500 is needed to converge to a low-concentration limit. The hydrophobic length of the peptide is slightly smaller than that of the shortest CG3 lipid, and the strength of the negative hydrophobic mismatch increases as the lipid thickness increases. Lipid sorting follows the predicted trend, with consistent moderate enrichment of shorter-tailed lipids near the peptide. A notable dependence of the degree of lipid sorting on system size is evident, with the local composition deviating from the bulk composition to an increasing degree as the ratio increases from 128:1 to 500:1. This trend, and the gradual change in composition over several layers of lipids surrounding the protein shown in Fig. 2, contrast with the findings of Powl et al. (11) and with their conclusion that composition is only perturbed among the immediate annulus of lipids neighboring the helix-bundle protein MscL. Although this discrepancy may point to shortcomings of the simulation model or to a high level of system specificity in lipid sorting response to hydrophobic mismatch, a more interesting interpretation is that the proteins observed experimentally cluster closely together with their lipid annuli touching or overlapping, as observed in recent CG simulations of membrane proteins under negative hydrophobic mismatch conditions (40,41).

In atomistic model simulations, the OmpA peptide was studied in both DMPC-DDPC and DSPC-DMPC lipid bilayers, corresponding to CG4-CG3 and CG5-CG4 lipid bilayers in MARTINI. In the three trajectories performed for each lipid mixture, sensitivity to initial conditions was evident. At both lipid compositions, one of three trajectories produced a β-barrel filled with solvent, and in another DMPC-DDPC run, a pore appeared in the bilayer adjacent to the peptide. Local thinning was observed in five of six trajectories, and weak lipid sorting effects (similar in magnitude to the CG model results) were seen in four of those five cases. We conclude that CG and atomistic models (in particular, the MARTINI force field and the Berger UA force fields) capture the same interplay of packing, elasticity, and entropic effects that lead to weak lipid sorting according to tail length under negative hydrophobic mismatch conditions, with the range of composition variations extending >2 nm from the surface of the peptide. Finally, the influence of the peptide on the lipid tail order parameters yielded some counterintuitive results, i.e., local thinning of the bilayer was associated with an increase in tail order. These cases can be explained by considering the full thickness profile of the system: ordering associated with bilayer thickening at intermediate distances from the peptide may counterbalance disordering at short distances.

SUPPORTING MATERIAL

A figure is available at http://www.biophysj.org/biophysj/supplemental/S0006-3495(12)00447-X.

This material is based in part on work supported by the National Science Foundation under grant number CHE-0911285. This work used TeraGrid resources provided by the Texas Advanced Computing Center, and computational resources of the Cherry Emerson Center for Scientific Computation, supported by the National Science Foundation's MRI-R2 program (CHE-0958205).

REFERENCES

1. Jensen, M. Ø., and O. G. Mouritsen. 2004. Lipids do influence protein function-the hydrophobic matching hypothesis revisited. *Biochim. Biophys. Acta.* 1666:205–226.
2. Andersen, O. S., and R. E. Koeppe, 2nd. 2007. Bilayer thickness and membrane protein function: an energetic perspective. *Annu. Rev. Biophys. Biomol. Struct.* 36:107–130.
3. Nyholm, T. K. M., S. Özdirekcan, and J. A. Killian. 2007. How protein transmembrane segments sense the lipid environment. *Biochemistry.* 46:1457–1465.
4. Dumas, F., M. C. Lebrun, and J.-F. Tocanne. 1999. Is the protein/lipid hydrophobic matching principle relevant to membrane organization and functions? *FEBS Lett.* 458:271–277.
5. Dumas, F., M. M. Sperotto, …, O. G. Mouritsen. 1997. Molecular sorting of lipids by bacteriorhodopsin in dilauroylphosphatidylcholine/distearoylphosphatidylcholine lipid bilayers. *Biophys. J.* 73: 1940–1953.
6. Ridder, A. N., R. E. J. Spelbrink, …, J. A. Killian. 2004. Photo-cross-linking analysis of preferential interactions between a transmembrane peptide and matching lipids. *Biochemistry.* 43:4482–4489.
7. Caffrey, M., and G. W. Feigenson. 1981. Fluorescence quenching in model membranes. 3. Relationship between calcium adenosinetriphosphatase enzyme activity and the affinity of the protein for phosphatidylcholines with different acyl chain characteristics. *Biochemistry.* 20:1949–1961.
8. Webb, R. J., J. M. East, …, A. G. Lee. 1998. Hydrophobic mismatch and the incorporation of peptides into lipid bilayers: a possible mechanism for retention in the Golgi. *Biochemistry.* 37:673–679.
9. O'Keeffe, A. H., J. M. East, and A. G. Lee. 2000. Selectivity in lipid binding to the bacterial outer membrane protein OmpF. *Biophys. J.* 79:2066–2074.
10. Mall, S., R. Broadbridge, …, J. M. East. 2000. Effects of aromatic residues at the ends of transmembrane α-helices on helix interactions with lipid bilayers. *Biochemistry.* 39:2071–2078.
11. Powl, A. M., J. M. East, and A. G. Lee. 2007. Different effects of lipid chain length on the two sides of a membrane and the lipid annulus of MscL. *Biophys. J.* 93:113–122.
12. Marsh, D. 2008. Energetics of hydrophobic matching in lipid-protein interactions. *Biophys. J.* 94:3996–4013.
13. Nielsen, S. O., C. F. Lopez, …, M. L. Klein. 2004. Transmembrane peptide-induced lipid sorting and mechanism of Lα-to-inverted phase transition using coarse-grain molecular dynamics. *Biophys. J.* 87: 2107–2115.

14. Klingelhoefer, J. W., T. Carpenter, and M. S. P. Sansom. 2009. Peptide nanopores and lipid bilayers: interactions by coarse-grained molecular-dynamics simulations. *Biophys. J.* 96:3519–3528.

15. Monticelli, L., S. K. Kandasamy, …, S.-J. Marrink. 2008. The MARTINI coarse-grained force field: extension to proteins. *J. Chem. Theory Comput.* 4:819–834.

16. de Joannis, J., Y. Jiang, …, J. T. Kindt. 2006. Equilibrium distributions of dipalmitoyl phosphatidylcholine and dilauroyl phosphatidylcholine in a mixed lipid bilayer: atomistic semigrand canonical ensemble simulations. *J. Phys. Chem. B.* 110:25875–25882.

17. Kindt, J. T. 2011. Atomistic simulation of mixed-lipid bilayers: mixed methods for mixed membranes. *Mol. Simul.* 37:516–524.

18. Yin, F., and J. T. Kindt. 2010. Atomistic simulation of hydrophobic matching effects on lipid composition near a helical peptide embedded in mixed-lipid bilayers. *J. Phys. Chem. B.* 114:8076–8080.

19. Pautsch, A., and G. E. Schulz. 1998. Structure of the outer membrane protein A transmembrane domain. *Nat. Struct. Biol.* 5:1013–1017.

20. Marrink, S. J., H. J. Risselada, …, A. H. de Vries. 2007. The MARTINI force field: coarse grained model for biomolecular simulations. *J. Phys. Chem. B.* 111:7812–7824.

21. Hess, B., C. Kutzner, …, E. Lindahl. 2008. GROMACS 4: algorithms for highly efficient, load-balanced, and scalable molecular simulation. *J. Chem. Theory Comput.* 4:435–447.

22. Periole, X., M. Cavalli, …, M. A. Ceruso. 2009. Combining an elastic network with a coarse-grained molecular force field: structure, dynamics, and intermolecular recognition. *J. Chem. Theory Comput.* 5:2531–2543.

23. Berendsen, H. J. C., J. P. M. Postma, …, J. R. Haak. 1984. Molecular dynamics with coupling to an external bath. *J. Chem. Phys.* 81:3684–3690.

24. Rzepiela, A. J., L. V. Schäfer, …, S. J. Marrink. 2010. Reconstruction of atomistic details from coarse-grained structures. *J. Comput. Chem.* 31:1333–1343.

25. Jorgensen, W. L., and J. Tirado-Rives. 1988. The OPLS [optimized potentials for liquid simulations] potential functions for proteins, energy minimizations for crystals of cyclic peptides and crambin. *J. Am. Chem. Soc.* 110:1657–1666.

26. Berger, O., O. Edholm, and F. Jähnig. 1997. Molecular dynamics simulations of a fluid bilayer of dipalmitoylphosphatidylcholine at full hydration, constant pressure, and constant temperature. *Biophys. J.* 72:2002–2013.

27. Jorgensen, W. L., J. Chandrasekhar, …, M. L. Klein. 1983. Comparison of simple potential functions for simulating liquid water. *J. Chem. Phys.* 79:926–935.

28. Tieleman, D. P., J. L. Maccallum, …, L. Monticelli. 2006. Membrane protein simulations with a united-atom lipid and all-atom protein model: lipid-protein interactions, side chain transfer free energies and model proteins. *J. Phys. Condens. Matter.* 18:S1221–S1234.

29. van Gunsteren, W. F., and H. J. C. Berendsen. 1988. A leap-frog algorithm for stochastic dynamics. *Mol. Simul.* 1:173–185.

30. Essman, U., L. Perera, …, L. G. Pedersen. 1995. A smooth particle mesh Ewald method. *J. Chem. Phys.* 103:8577–8592.

31. Miyamoto, S., and P. A. Kollman. 1992. SETTLE: an analytical version of the SHAKE and RATTLE algorithms for rigid water models. *J. Comput. Chem.* 13:952–962.

32. Hess, B., H. Bekker, …, J. G. E. M. Fraaije. 1997. LINCS: a linear constraint solver for molecular simulations. *J. Comput. Chem.* 18:1463–1472.

33. Siepmann, J. I., and D. Frenkel. 1992. Configurational bias Monte Carlo: a new sampling scheme for flexible chains. *Mol. Phys.* 75:59–70.

34. Humphrey, W., A. Dalke, and K. Schulten. 1996. VMD: visual molecular dynamics. *J. Mol. Graph.* 14:33–38, 27–28.

35. Brannigan, G., and F. L. H. Brown. 2006. A consistent model for thermal fluctuations and protein-induced deformations in lipid bilayers. *Biophys. J.* 90:1501–1520.

36. Marrink, S. J., A. H. de Vries, and A. E. Mark. 2004. Coarse grained model for semiquantitative lipid simulations. *J. Phys. Chem. B.* 108:750–760.

37. Brannigan, G., and F. L. H. Brown. 2005. Composition dependence of bilayer elasticity. *J. Chem. Phys.* 122:074905.

38. Gil, T., J. H. Ipsen, …, M. J. Zuckermann. 1998. Theoretical analysis of protein organization in lipid membranes. *Biochim. Biophys. Acta.* 1376:245–266.

39. Mall, S., R. Broadbridge, …, A. G. Lee. 2001. Self-association of model transmembrane α-helices is modulated by lipid structure. *Biochemistry.* 40:12379–12386.

40. Schmidt, U., and M. Weiss. 2010. Hydrophobic mismatch-induced clustering as a primer for protein sorting in the secretory pathway. *Biophys. Chem.* 151:34–38.

41. Parton, D. L., J. W. Klingelhoefer, and M. S. P. Sansom. 2011. Aggregation of model membrane proteins, modulated by hydrophobic mismatch, membrane curvature, and protein class. *Biophys. J.* 101: 691–699.

42. Mouritsen, O. G., and M. Bloom. 1993. Models of lipid-protein interactions in membranes. *Annu. Rev. Biophys. Biomol. Struct.* 22:145–171.

43. Wang, H., J. de Joannis, …, J. T. Kindt. 2008. Bilayer edge and curvature effects on partitioning of lipids by tail length: atomistic simulations. *Biophys. J.* 95:2647–2657.

44. Bond, P. J., J. D. Faraldo-Gómez, and M. S. P. Sansom. 2002. OmpA: a pore or not a pore? Simulation and modeling studies. *Biophys. J.* 83:763–775.

45. Smith, S. G. J., V. Mahon, …, R. P. Fagan. 2007. A molecular Swiss army knife: OmpA structure, function and expression. *FEMS Microbiol. Lett.* 273:1–11.

46. Hong, H., and L. K. Tamm. 2004. Elastic coupling of integral membrane protein stability to lipid bilayer forces. *Proc. Natl. Acad. Sci. USA.* 101:4065–4070.

47. Hong, H., G. Szabo, and L. K. Tamm. 2006. Electrostatic couplings in OmpA ion-channel gating suggest a mechanism for pore opening. *Nat. Chem. Biol.* 2:627–635.

48. Zakharian, E., and R. N. Reusch. 2005. Kinetics of folding of *Escherichia coli* OmpA from narrow to large pore conformation in a planar bilayer. *Biochemistry.* 44:6701–6707.

49. Ellena, J. F., P. Lackowicz, …, D. S. Cafiso. 2011. Membrane thickness varies around the circumference of the transmembrane protein BtuB. *Biophys. J.* 100:1280–1287.